AD_____

Award Number: W81XWH-11-1-0372

TITLE: Intracellular Protein Delivery for Treating Breast Cancer

PRINCIPAL INVESTIGATOR: Pin Wang

CONTRACTING ORGANIZATION: University of Southern California

REPORT DATE: June 2012

TYPE OF REPORT: Annual

PREPARED FOR: U.S. Army Medical Research and Materiel Command
                          Fort Detrick, Maryland 21702-5012

REPORT DOCUMENTATION PAGE

Form Approved
OMB No. 0704-0188

Public reporting burden for this collection of information is estimated to average 1 hour per response, including the time for reviewing instructions, searching existing data sources, gathering and maintaining the data needed, and completing and reviewing this collection of information. Send comments regarding this burden estimate or any other aspect of this collection of information, including suggestions for reducing this burden to Department of Defense, Washington Headquarters Services, Directorate for Information Operations and Reports (0704-0188), 1215 Jefferson Davis Highway, Suite 1204, Arlington, VA 22202-4302. Respondents should be aware that notwithstanding any other provision of law, no person shall be subject to any penalty for failing to comply with a collection of information if it does not display a currently valid OMB control number. **PLEASE DO NOT RETURN YOUR FORM TO THE ABOVE ADDRESS.**

1. REPORT DATE 1Jun 2012	2. REPORT TYPE Annual	3. DATES COVERED 15 May 2011 to 14 May 2012

4. TITLE AND SUBTITLE	5a. CONTRACT NUMBER
Intracellular Protein Delivery for treating Breast Cancer	
	5b. GRANT NUMBER W81XWH-11-1-0372
	5c. PROGRAM ELEMENT NUMBER

6. AUTHOR(S)	5d. PROJECT NUMBER
Pin Wang	
	5e. TASK NUMBER
	5f. WORK UNIT NUMBER
E-Mail: yitang@ucla.edu	

7. PERFORMING ORGANIZATION NAME(S) AND ADDRESS(ES)	8. PERFORMING ORGANIZATION REPORT NUMBER
University of Southern California Los Angeles, CA 90089-0701	

9. SPONSORING / MONITORING AGENCY NAME(S) AND ADDRESS(ES)	10. SPONSOR/MONITOR'S ACRONYM(S)
U.S. Army Medical Research and Materiel Command Fort Detrick, Maryland 21702-5012	
	11. SPONSOR/MONITOR'S REPORT NUMBER(S)

12. DISTRIBUTION / AVAILABILITY STATEMENT
Approved for Public Release; Distribution Unlimited

13. SUPPLEMENTARY NOTES

14. ABSTRACT

The development of stimuli-responsive, nano-scale therapeutics that can selectively target tumors is a major research focus in cancer nanotechnology. A potent therapeutic option is directly arming the cancer cells with apoptotic-inducing proteins that are not targeted by anti-apoptotic maneuvers found in tumors. The avian virus derived apoptin forms a high molecular weight protein complex that selectively accumulates in the nuclei of cancer cells to induce apoptotic cell death. To enable the efficient delivery of this tumor-selective complex in functional form, we synthesized degradable, sub-100 nm, core-shell protein nanocapsules containing the 2.4 MDa apoptin complexes. Recombinant apoptin is reversibly encapsulated in a positively charged, water soluble polymeric shell and is released in native forms in response to reducing conditions such as the cytoplasm. The nanocapsules are efficiently internalized by mammalian cells lines as characterized by confocal microscopy, and rhodamine-labeled apoptin can be observed in the nuclei of cancer cells only. Released apoptin induced tumor-specific apoptosis in several cell lines and inhibited tumor growth in vivo, demonstrating the potential of this polymer-protein combination as a cancer therapeutic.

15. SUBJECT TERMS

Nanogels, core-shell, redox-responsive, apoptosis, breast cancer.

16. SECURITY CLASSIFICATION OF:			17. LIMITATION OF ABSTRACT	18. NUMBER OF PAGES	19a. NAME OF RESPONSIBLE PERSON USAMRMC
a. REPORT U	b. ABSTRACT U	c. THIS PAGE U	UU	25	19b. TELEPHONE NUMBER *(include area code)*

Table of Contents

INTRODUCTION

Specific induction of cell death in tumors is considered one of the most desired and effective anticancer therapies. Effective strategies to activate the apoptotic pathway, or other death mechanisms, are currently being intensely pursued. A potent chemotherapy option is directly arming the cancer cells with executioner proteins or apoptotic-inducing proteins that are not targeted by anti-apoptotic maneuvers found in many tumors. In this proposal, we will develop a new method to treat breast cancer by using a native-protein delivery approach. This is a platform to deliver proteins in native forms into cells. The key design feature of our strategy is to first encapsulate protein molecules in a thin layer of water soluble, positively charged, degradable polymer to form nanometer-sized nanocapsules. The nanocapsule shell facilitates uptake of the protein content into cells, and protects the protein both during in vivo circulation and endocytosis. To endow the nanocapsules biodegradability once entered the target cells, the polymer shell is crosslinked with redox-sensitive crosslinkers that can be reduced upon encountering the reducing environment of the cytoplasm. Our overall research objective is to thoroughly evaluate this delivery method as a potentially new therapeutic modality for breast cancer treatment. Three aims will be pursued in parallel and results from each aim will be used to guide the refinement of other aims and the overall research objective. 1) Delivering different target proteins to breast cancer cell lines using this approach, including the tumor specific apoptin; 2) Equipping the protein nanocapsules with specific cancer cell targeting ligands; 3) Examining the in vivo potency and pharmacokinetics of the nanocapsules.

BODY

Summary of State of Work

Specific Aim 1: Delivering different target proteins to breast cancer cell lines using protein nanocapsules
Task 1. Preparing and characterizing of Apoptin contained nanocapsules
This task has been completed. Detailed description can be found in the following pages.

Task 2. *in vitro* studying Apoptin contained nanocapsules
This task has been completed. Detailed description can be found in the following pages.

Specific Aim 2: Equipping protein nanocapsules with specific cancer cell targeting ligands;
Task 3. Preparing and testing of MMP activatable cell penetrating peptides (ACCPs)-coupled nanocapsules
This task is currently under evaluation, no results to report at this point.

Task 4. Preparing and testing of ligand-receptor affinity based targeting: Transferrin (Tf) and Herceptin
This task is currently under evaluation, no results to report at this point.

Specific Aim 3: Examining the *in vivo* potency and pharmacokinetics of the nanocapsules.

Task 5. Evaluating *in vivo* distribution of protein nanocapsules
This task has been partially performed and some results will be in the following pages.

Task 6. Examining the *in vivo* pharmacokinetics of nanocapsules
This task is currently under evaluation, no results to report at this point.

Task 7. Determing the *in vivo* delivery efficacy of nanocapsules
This task has been completed. Detailed description can be found in the following pages.

The following results have been submitted for publication and have been reformatted here. The submitted manuscript is attached in APPENDIX.

Background and Motivation

Intracelluar delivery of recombinant proteins for cancer therapy   The most desirable cancer therapy is both potent and specific towards tumor cells (Gibbs 2000; Atkins and Gershell 2002). Many conventional small molecule chemotheraputics do not discriminate between cancerous and normal cells, cause undesirable damage to healthy tissues, and are therefore unable to be administered at high dosage. In contrast, cytoplasmic and nuclear proteins that selectively alter the signaling pathways in tumor cells, reactivate apoptosis and restore tissue homeostasis, can eradicate cancerous cells and delay tumor progression with less collateral damage to other tissues (Evan and Vousden 2001; Reed 2003; Cotter 2009). Intracellular delivery of such proteins, including human tumor suppressors (such as p53) (Brown, Lain et al. 2009) and exogenous tumor-killing proteins (such as apoptin) (Backendorf, Visser et al. 2008), in their functional forms is attractive as a new anti-cancer therapy modality.

Apoptin   Apoptin is a small protein (121 amino acids) from chicken anemia virus (CAV) that induces p53-independent apoptosis in a tumor-specific way (Backendorf, Visser et al. 2008). In a variety of tumor cell lines, Apoptin becomes phosphorylated, enters the nucleus, and induces apoptosis (Zhuang, Shvarts et al. 1995; Danen-Van Oorschot, Fischer et al. 1997; Danen-Van Oorschot, Zhang et al. 2003). In sharp contrast, Apoptin is unphosphorylated in normal cells and stays in the cytoplasm. An important feature of Apoptin is that it can recognize early stages of oncogenesis and it can induce apoptosis. Currently known Apoptin targets include DEDAF, Nur77, Nmi, and Hippi, some of which are p53-independent signaling proteins in the apoptotic pathway (Backendorf, Visser et al. 2008). Due to its high selectivity and potency, Apoptin has become an attractive antitumor target for gene therapy approaches. For example, in a nude mouse model, injection of Apoptin-encoding adenoviruses to the site of breast carcinoma xenografts resulted in a significant reduction in tumor growth. Furthermore, Apoptin has been shown to be a safe agent, resulting in minimal toxicity and weight loss in mouse models. Recombinant Apoptin expressed by *E. coli* can induce rapid apoptosis in cancer cells when microinjected into tumor cells (Leliveld, Zhang et al. 2003). In comparison, no apoptosis was observed in normal cells. Moreover, when fused to the HIV-TAT protein transduction domain, TAT-Apoptin was transduced efficiently into normal and tumor cells. However, TAT-Apoptin remained in the cytoplasm and did not kill normal 6689 and 1BR3 fibroblasts. In contrast, TAT-Apoptin migrated from the cytoplasm to the nucleus of Saos-2 and HSC-3 cancer cells resulting in apoptosis after 24 h (Guelen, Paterson et al. 2004). These results indicate that recombinant Apoptin captures all of the essential functions and selectivity of the native protein. Therefore, Apoptin is an excellent target for expanding the applications of nanocapsules as a chemotherapy modality.

Task 1: Preparing and characitizing of Apoptin-contained nanocapsules

MBP-APO synthesis: As shown in Figure 1, we chose to work with maltose-binding-protein fused apoptin (MBP-APO), which can be easily expressed in soluble form by bacterial E. coli. We obtained the pMalTBVp3 plasmid for expression of the MBP-APO from colleagues at Universiteit Leiden. MBP-APO plasmid was transformed into E. coli BL21(DE3) cells for recombinant protein expression. After overnight incubation at 16 °C, the cells were harvested by centrifugation. Cell pellets were then be resuspended in lysis buffer and lysed by sonication. Cell debries and insoluble proteins were removed by centrifugation followed by filtering through 0.22 um filters to fully clear cell lysate. The protein was
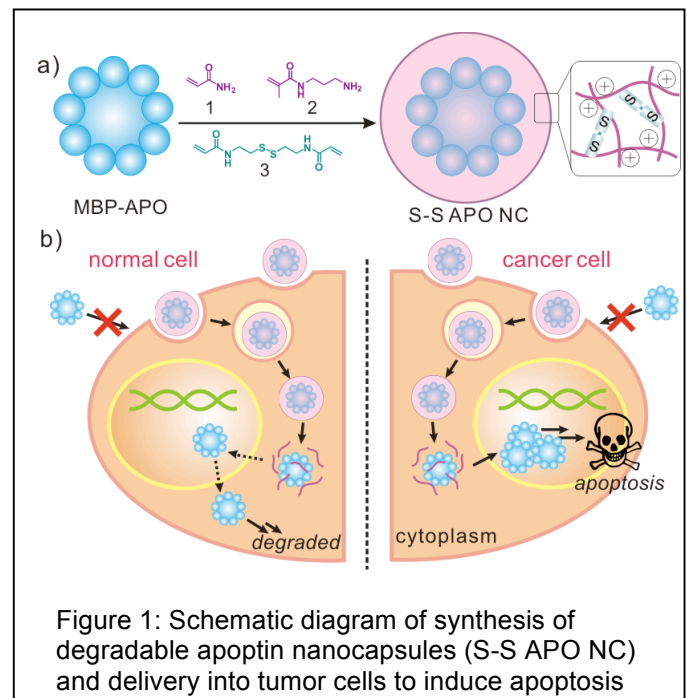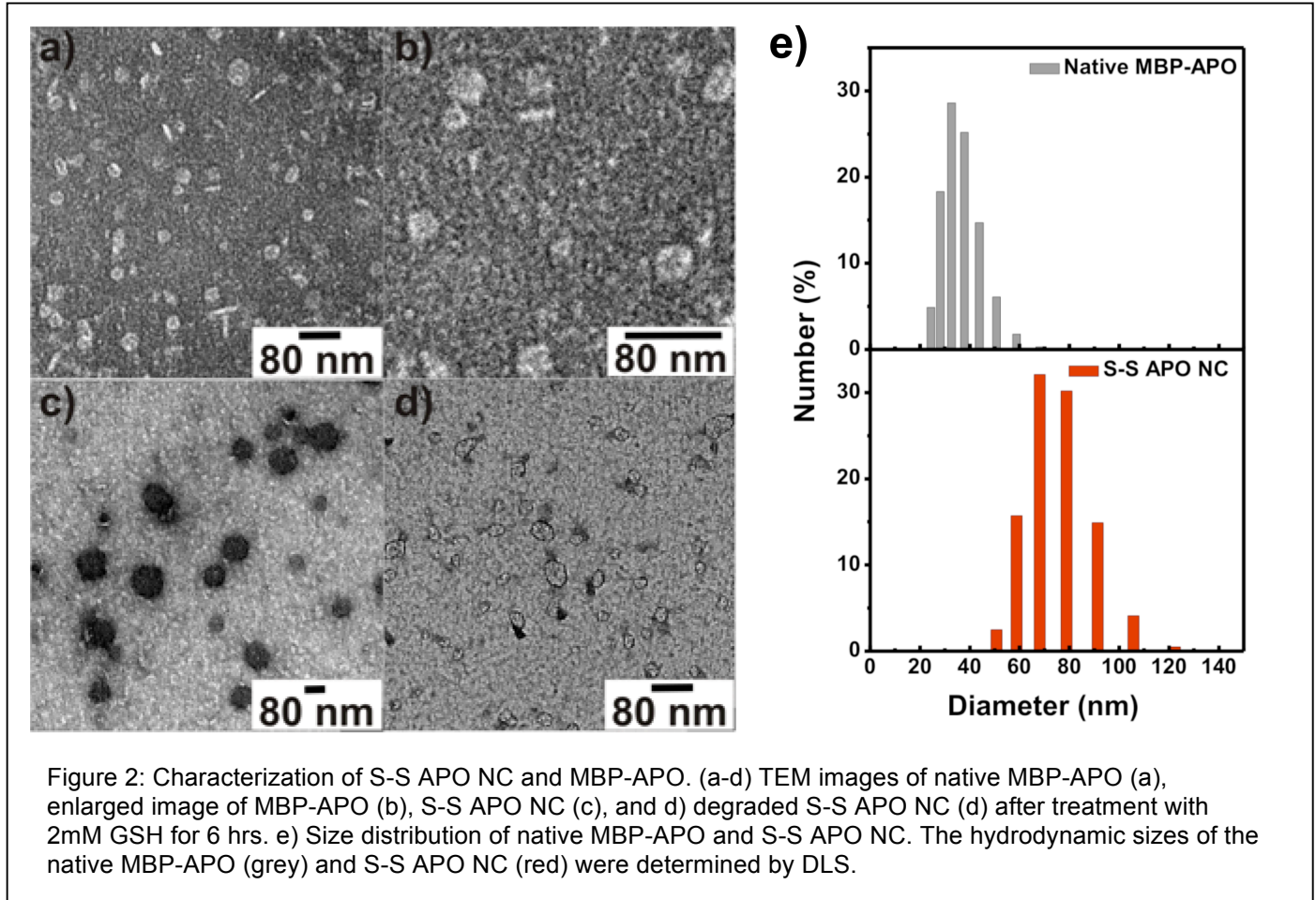

Figure 1: Schematic diagram of synthesis of degradable apoptin nanocapsules (S-S APO NC) and delivery into tumor cells to induce apoptosis

then purified by an amylase column and MBP-APO was eluted from the column and buffer exchanged into PBS.

Nanocapsule preparation: The MBP-APO protein was diluted to 1 mg/mL with 5 mM sodium bicarbonate buffer at pH 9. Then 200 mg/mL acrylamide (AAm) monomer was added to 1 mL of protein solution with stirring at 4 °C. After 10 min, the second monomer, *N*-(3-aminopropyl) methacrylamide (APMAAm), was added while stirring. Different cross-linkers, *N,N'*-methylene bisacrylamide for ND NC and *N,N'*-bis(acryloyl)cystamine for S-S NC, was added 5 min after the addition of APMAAm. The polymerization reaction was immediately initiated by adding 30 µL of ammonium persulfate (100 mg/mL, dissolved in deoxygenated and deionized water) and 3 µL of *N,N,N',N'*-tetramethylethylenediamine. The polymerization reaction was allowed to proceed for 60 min. The molar ratio of AAm/APMAAm/cross-linker was adjusted to 12:9:1. Buffer exchange with phosphate-buffered saline (PBS) buffer (pH 7.4) was used to remove the

Figure 2: Characterization of S-S APO NC and MBP-APO. (a-d) TEM images of native MBP-APO (a), enlarged image of MBP-APO (b), S-S APO NC (c), and d) degraded S-S APO NC (d) after treatment with 2mM GSH for 6 hrs. e) Size distribution of native MBP-APO and S-S APO NC. The hydrodynamic sizes of the native MBP-APO (grey) and S-S APO NC (red) were determined by DLS.
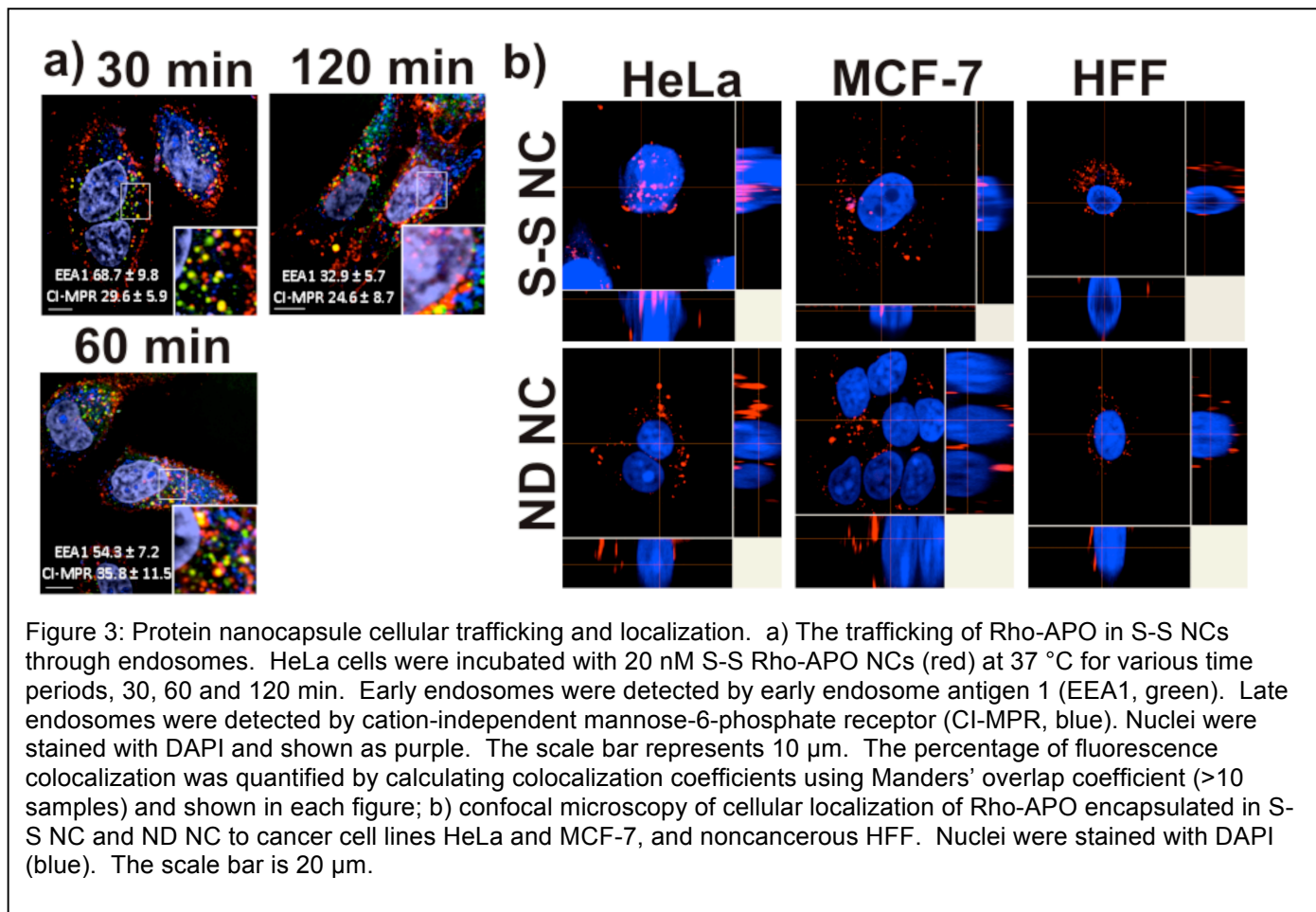
remaining monomers and initiators. For tracking MBP-APO nanocapsules, we also prepared Rhodamine-tagged MBP-APO nanocapsules, which were obtained through encapsulation of MBP-APO modified with 5-Carboxy-X-rhodamine *N*-succinimidyl ester (mass ratio (MBP-APO: rhodamine): 4:1).

Characterization of MBP-APO and its nanocapsule form: The mean hydrodynamic size and zeta potential of nanocapsules were determined by dynamic light scattering (DSL). DSL measurement revealed an average hydrodynamic radius of 36.1 nm (distribution shown in Figure 2e), consistent with that of the reported for the MBP-APO complex. Transmission Electron Microscopy (TEM) analysis of MBP-APO showed similarly sized protein complexes (Figure 2a and enlarged in Figure 2b). Interestingly, MBP-APO complexes appear to adopt a disk-shaped structure despite the lack of defined secondary structure from the apoptin component. Since the apoptin portion of the protein can self-assemble into the ~40-mer complex, we propose a three dimensional arrangement of MBP-APO in which the *C*-terminal apoptin forms the central spoke of the wheel-like structure (Figure 1), with the larger MBP portion distributed around on the edge. The planar arrangement allows the apoptin portion of the fusion protein to remain accessible to its protein partners, which may explain how the MBP-APO fusion retains essentially all of the observed functions of free apoptin.

The DSL measurement of the nanocapsule form of MBP-APO (termed S-S APO NC) clearly showed increase in average diameter of the sample to ~ 75 nm with a slightly positive ζ-potential value of 2.4 mV. TEM

analysis of the S-S NC confirmed the nearly doubling in diameter of the spherical particle (Figure 2c). Unexpectedly, the NCs displayed dark contrast upon uranyl acetate staining not typically observed with polymeric particles, which hints the cores of the particles are very densely packed. As expected of the redox-responsive crosslinkers, the reduction of nanocapsule size to essentially that of the native MBP-APO can be seen upon treatment of the reducing agent glutathione (2 mM GSH, 6 hours 37°C). As shown in Figure 2d, the densely packed NCs were completely dissociated into particles (~30 nm) that resemble those seen in Figure 2a, confirming the reversible nature of the encapsulation process. In contrast, the densely packed MBP-APO nanocapsules crosslinked with the nondegradable crosslinker *N,N'*-methylene bisacrylamide (ND APO NC) were not degraded in the presence of GSH (data not shown).

Task 2: in vitro studying Apoptin-containing nanocapsules

Figure 3: Protein nanocapsule cellular trafficking and localization. a) The trafficking of Rho-APO in S-S NCs through endosomes. HeLa cells were incubated with 20 nM S-S Rho-APO NCs (red) at 37 °C for various time periods, 30, 60 and 120 min. Early endosomes were detected by early endosome antigen 1 (EEA1, green). Late endosomes were detected by cation-independent mannose-6-phosphate receptor (CI-MPR, blue). Nuclei were stained with DAPI and shown as purple. The scale bar represents 10 µm. The percentage of fluorescence colocalization was quantified by calculating colocalization coefficients using Manders' overlap coefficient (>10 samples) and shown in each figure; b) confocal microscopy of cellular localization of Rho-APO encapsulated in S-S NC and ND NC to cancer cell lines HeLa and MCF-7, and noncancerous HFF. Nuclei were stained with DAPI (blue). The scale bar is 20 µm.

Cellular uptake and localization: We next examined the cellular uptake of the S-S APO NC and its cellular localization. If the unique tumor selectivity of MBP-APO is maintained following the encapsulation and releases processes, we expect to find MBP-APO to enter the nucleus of the tumor cell, whereas in noncancerous cell it resides in the cytoplasm. Prior to the polymerization process, the native MBP-APO was conjugated to amine-reactive rhodamine (Rho-APO). Subsequent encapsulation yielded similarly sized nanocapsules. MDA-MB-231 breast tumor cells were seeded into 48-well plate. Once the confluency of 80% was reached, S-S Rho-APO NC and ND Rho-APC NC were added to a final concentration of 20 nM. Fluorescent images showed all NCs readily penetrated the cell membrane and can be observed to be localized in the cytoplasm within one hour (Figure 3a).

To determine the cellular localization of delivered proteins, confocal images were taken with HeLa, MCF-7, or HEF cells incubated with 20 nM of S-S Rho-APO NC or ND-Rho-APO NC at 37 °C for 24 hrs. Nuclei were then counterstained with DAPI. The Z stack images of cells were imaged at 0.4-µm intervals and analyzed by Nikon NIS Element software. Fluorescence images were acquired on a Yokogawa spinning-disk confocal scanner system using a Nikon eclipse Ti-E microscope equipped with a 60×/1.49 Apo TIRF oil objective and a Cascade II: 512 EMCCD camera. As cytotoxicity was observed with the cancer cell lines treated with S-S APO NC (see Figure 4), sub-lethal concentrations (20 nM) of the NCs were added to imaging

samples and the cells were collected before morphology changed and detachment took place. In the case of ND Rho-APO NCs, red fluorescence signals remained in the cytoplasm for all three cell lines, indicating the MBP-APO was well-shielded by the nondegradable polymeric shell and its nuclear localization signals is not accessible. In stark contrast, when HeLa cells were treated with S-S Rho-APO NC, strong red fluorescence of rhodamine was localized in the nuclei, resulting in intense pink color as a result of overlapping of rhodamine and DAPI fluroescence. Z-stacking analysis confirmed the MBP-APO to be localized inside of the nuclei (Figure 3b). Similar results were observed with MCF7 cells, although the fluorescence intensity was not as strong as in the HeLa cells. These results confirmed that the MBP-APO delivered can indeed be released in native forms inside the cytoplasm and enter the nuclei. More importantly, the specificity of MBO-APO delivered towards cancer cell lines were demonstrated in the confocal image of noncancerous HFF cells treated with S-S Rho-APO NC, as all of the dye signals remained in the cytosol and no nuclear accumulation can be observed.
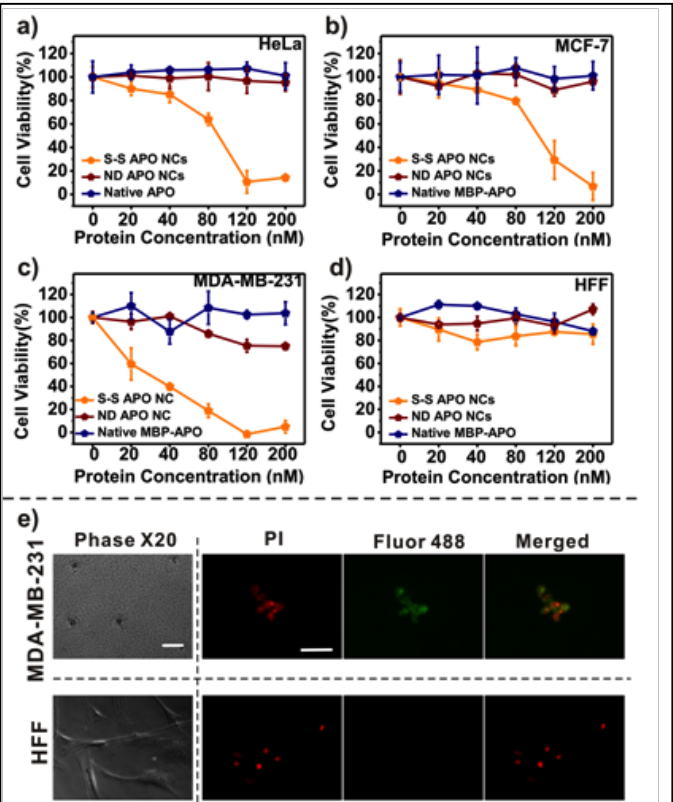

Figure 4: Cytotoxicity and apoptosis observed following S-S APO NC treatment. (a) HeLa; (b) MCF-7; (c) MDA-MB-231; or (d) HFF cells with treatment of different concentrations of S-S APO NC, ND APO NC, and native MBP-APO (e) Apoptosis induced by S-S APO NC determined by TUNEL assay.

Cytotoxicity study: We then investigated whether the MBP-APO protein delivered still possess its function to induce tumor-selective apoptosis. The potency and selectivity of S-S APO NCs was tested on cancer cell lines HeLa, MCF-7, MDA-MB-231, and the HFF (Figure 4a). These cells were seeded into 96-well plates, each well containing 5,000 cells in 100 µL of DMEM with supplements.   Different concentrations of protein and NCs were added into each well and the plates were incubated at 37 °C with 98 % humidity and 5 % CO_2 for 48 hours. The cells were washed with PBS solution twice and 100 µL of fresh cell culture media with supplements was added. Then 20 µL MTS solution was added into each well and the plates were incubated for 3 hours at 37 °C. The absorbance of product was read at 490 nm using a microplate reader. For each cell line, ND APO NC and native MBP-APO were used as negative controls. When S-S APO NC was added to a final concentration of 200 nM, all three cancer cell lines had no viable cells, whereas remarkably ~75 % of the HFF had survived. The IC_{50} values were 80 and 30 nM for HeLa and MDA-MB-231, respectively. The IC_{50} for MCF-7 was notably higher at ~100 nM, which may be due to the deficiency in the terminal executioner CP-3 and reliance on other effector caspases for apoptosis. As expected, native MBP-APO and ND APO NC did not notably decrease the viability of any these cell lines tested, consistent with the inability to enter cells and release MBP-APO, respectively. The morphologies of MDA-MB-231 and HFF cells were examined under after the various treatments. Only the S-S MBP-APO NC treated MDA-MB-231 cells exhibited blebbing and shrinkage, which are hallmarks of apoptotic cell death (Figure 4b). Using TUNEL assay, only S-S MBP-APO NC treated MDA-MB-231 showed
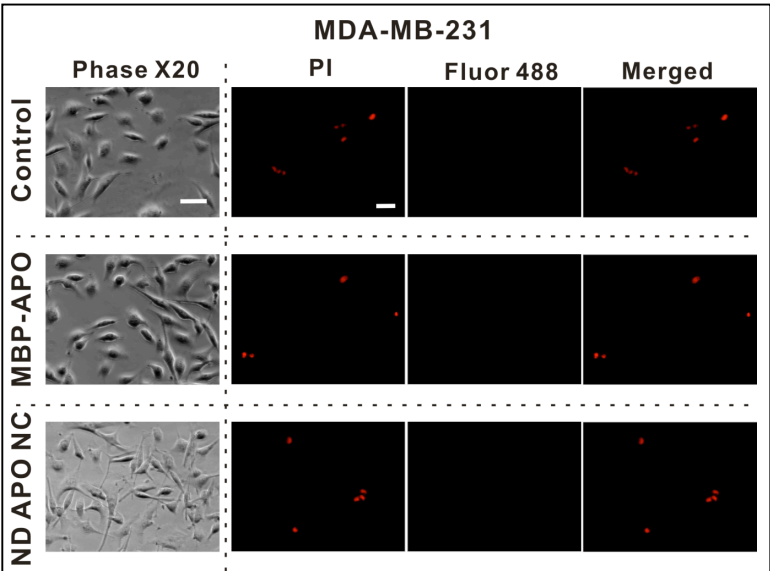

Figure 5: MDA-MB-231 cells TUNEL assay.

nuclear fragmentation associated with apoptosis (Fluor 488), whereas all other samples, native MBP-APO, ND

APO NC at the same concentration, as well as HFF treated with 200 nM S-S APO NC had no sign of apoptosis (Figure 5). Collectively, these results demonstrate the released MBP-APO upon degradation retains the potency and selectivity as the transgenically expressed apoptin in previous studies.

Task 5: Evaluation in vivo biodistribution of protein nanocapsules
Task 7: Determining the in vivo delivery efficacy of nanocapsules

Xenograft and biodistribution study: We further examined its potency in mouse xenograft model. Female athymic nude (*nu/nu*) mice were subcutaneously grafted on the back flank with 5×10^6 MCF-7 breast cancer cells. When the tumor volume reached 100-200 mm^3 (day 0), mice were randomly separated into different groups and treated with intratumoral injection of PBS, MBP-APO, S-S APO NC. In addition, S-S BSA (bovine serum albumin) NC as added as a nonlethal protein cargo control testing the effects of the S-S NC capsule components on tumor cells in vivo. Tumors treated with saline or S-S BSA NC expanded rapidly and reached the maximum limit (>2500 mm^3) within 12 days (Figure 6a). In sharp contrast, tumor growth was significantly delayed when treated with S-S APO NC. The native MBP-APO showed negligible tumor inhibition in the treated group over time, which was consistent with the *in vitro* study results. Fixed tumor tissues collected from each treatment group were examined for DNA fragmentation using *in situ* TUNEL assay. The images revealed the highest level of cell apoptosis for the tumor harvested from mice treated with S-S APO NC (Figure 6b), correlating well with the significantly delayed tumor growth observed for this treatment group and confirming that tumor growth inhibition was indeed due to apoptin-mediated apoptosis. The observed high-degree apoptosis indicates that in addition to tumor cell killing directly caused by uptake of apoptin, the dying cells can lead to a possible bystander killing effect on surrounding tumor cells, which may increase overall therapeutic effect of S-S APO NC. The xenograft study verified that the S-S NC effectively delivered MBP-APO proteins to tumor cells *in vivo* and significantly slowed down tumor progression.
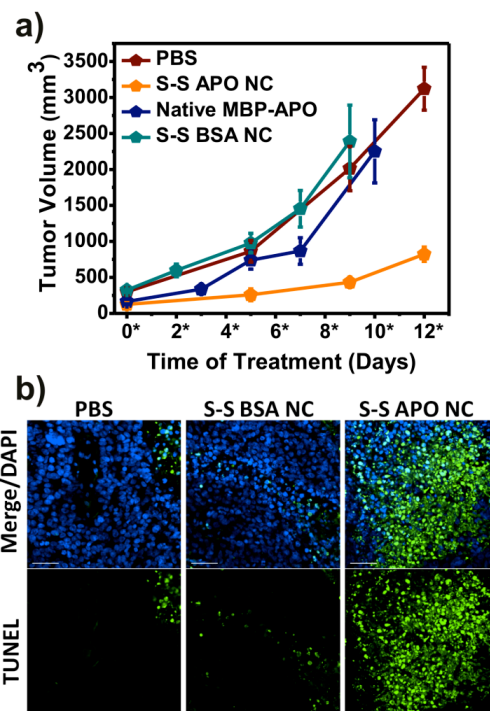

Figure 6: Treatment of S-S APO NC results in tumor growth retardation through apoptosis. (a) Tumor growth curves; (b) In situ apoptosis staining of tumor tissues

KEY RESEARCH ACCOMPLISHMENTS

1) We have successfully synthesized the Apoptin-encapsualted nanocapsules with desired nanostructure and biophysical properties.

2) In vitro internalization and intracellular trafficking studies reveal that such nanocapsules are able to be efficiently uptaken by cells and transported into nucleus.

3) In vitro cytotoxicity study shows that Apoptin-encapsulated nanocapsules can induce tumor-specific apoptosis.

4) The breast cancer xenograft study reveals that Apoptin nanocapsules can inhibit tumor growth in vivo.

REPORTABLE OUTCOMES

Publications:
The results above have been submitted for publication in *Nano Today*

Zhao, M., Hu, B., Gu, Z., Joo, K., Wang, P., Tang, Y. "Degradable Polymeric Nanocapsule for Efficient Intracellular Delivery of a High Molecular Weight Tumor-Selective Protein Complex." *Nano Today.* **2012**, *submitted*

Presentations:

The PI Wang has made the following presentations in which this material has been included.
AICHE Annual Meeting, Minneapolis, MN, October 2011
Ming Hsieh Symposium, University of Southern California, Los Angeles, September 2011

The following poster presentation was made at the American Association for Cancer Research Special Conference: Molecular Targets and Cancer Therapeutics. November 12-16, 2011, San Francisco

"Delivery of tumor killing protein to cancer cells." Muxun Zhao, Biliang Hu, Pin Wang, Yi Tang. University of California, Los Angeles, Los Angeles, CA; University of Southern California, Los Angeles, CA

CONCLUSION

We were able to deliver the high molecular weight complex of the tumor-selective MBP-APO using a redox-responsive polymeric nanocapsule *in vitro* and *in vivo*. The choice and design of the sub-100 nm nanocapsule is well-suited for diverse protein targets because of its mild preparation conditions, completely reversible encapsulation and efficient cell membrane penetration/release of the protein cargo in the cytoplasm. Our application here further illustrates how intracellular protein delivery using nanoscale system can provide new possibilities for achieving selective cancer therapy.

REFERENCES

Atkins, J. H. and L. J. Gershell (2002). "Selective anticancer drugs." Nat Rev Drug Discov 1(7): 491-492.

Backendorf, C., A. E. Visser, et al. (2008). "Apoptin: therapeutic potential of an early sensor of carcinogenic transformation." Annu Rev Pharmacol Toxicol 48: 143-169.

Brown, C. J., S. Lain, et al. (2009). "Awakening guardian angels: drugging the p53 pathway." Nat Rev Cancer 9(12): 862-873.

Cotter, T. G. (2009). "Apoptosis and cancer: the genesis of a research field." Nat Rev Cancer 9(7): 501-507.

Danen-Van Oorschot, A. A., D. F. Fischer, et al. (1997). "Apoptin induces apoptosis in human transformed and malignant cells but not in normal cells." Proc Natl Acad Sci U S A 94(11): 5843-5847.

Danen-Van Oorschot, A. A., Y. H. Zhang, et al. (2003). "Importance of nuclear localization of apoptin for tumor-specific induction of apoptosis." J Biol Chem 278(30): 27729-27736.

Evan, G. I. and K. H. Vousden (2001). "Proliferation, cell cycle and apoptosis in cancer." Nature 411(6835): 342-348.

Gibbs, J. B. (2000). "Mechanism-based target identification and drug discovery in cancer research." Science 287(5460): 1969-1973.

Guelen, L., H. Paterson, et al. (2004). "TAT-apoptin is efficiently delivered and induces apoptosis in cancer cells." Oncogene 23(5): 1153-1165.

Leliveld, S. R., Y. H. Zhang, et al. (2003). "Apoptin induces tumor-specific apoptosis as a globular multimer." J Biol Chem 278(11): 9042-9051.

Reed, J. C. (2003). "Apoptosis-targeted therapies for cancer." Cancer Cell 3(1): 17-22.

Zhuang, S. M., A. Shvarts, et al. (1995). "Apoptin, a protein derived from chicken anemia virus, induces p53-independent apoptosis in human osteosarcoma cells." <u>Cancer Res</u> 55(3): 486-489.

APPENDICES:

Efficient Delivery of a High Molecular Weight Tumor-Selective Protein Complex **

*Muxun Zhao, Biliang Hu, Zhen Gu, Kye-Il Joo, Pin Wang and Yi Tang**

The most desirable cancer therapy is both potent and specific towards tumor cells.[1,2] Many conventional small molecule chemotheraputics do not discriminate between cancerous and normal cells, cause undesirable damage to healthy tissues, and are therefore unable to be administered at high dosage. In contrast, cytoplasmic and nuclear proteins that selectively alter the signaling pathways in tumor cells, reactivate apoptosis and restore tissue homeostasis, can eradicate cancerous cells and delay tumor progression with less collateral damage to other tissues.[3-6] Intracellular delivery of such proteins, including human tumor suppressors (such as p53[7]) and exogenous tumor-killing[8] proteins (such as apoptin [9,10]), in their functional forms is attractive as a new anti-cancer therapy modality.

Apoptin is a 121-residue protein derived from chicken anemia virus.[9] When transgenically expressed, apoptin was shown to induce p53-independent apoptosis in a variety of tumor and transformed cells,[11,12] while leaving normal and untransformed cells unaffected.[13] Apoptin exists in a globular multimer complex of thirty to forty subunits with no well-defined secondary structure.[14] While the exact mechanism of the tumor selectivity is unresolved, apoptin is known to translocates to the nuclei where tumor-specific phosphorylation at residue Thr108 takes place, leading to accumulation of apoptin in nuclei and activation of the apoptotic cascade.[15] In normal cells, apoptin is not phosphorylated at Thr108 and is located mostly in the cytoplasm, where it becomes aggregated and degraded.[16] Because of the high potency in inducing this exquisite tumor-selective apoptosis, apoptin has been investigated widely as an anti-tumor therapeutic option.[9] Different gene therapy approaches have been used to administer apoptin to mouse xenograft tumor models, in which significant reduction in tumor sizes and prolong of mice lifespan have been observed without compromising the overall health.[17-19] However, as with

other gain-of-function therapy candidates, *in vivo* gene delivery approaches, such as the use of adenoviral vectors may lead to chromosomal modifications and raise safety concerns.[20] While protein transduction domain-fused apoptin has been delivery to cells,[21,22] this approach suffers from inefficient release of the cargo from endosomes and instability of the unprotected protein. Development of nanoparticle carriers to aid the delivery of functional forms of apoptin to tumor cells is therefore highly desirable.[23] Herein, we describe the efficient delivery of apoptin using a degradable polymeric nanocapsule to different cancer cell lines *in vitro* and to xenograft tumor model *in vivo*.
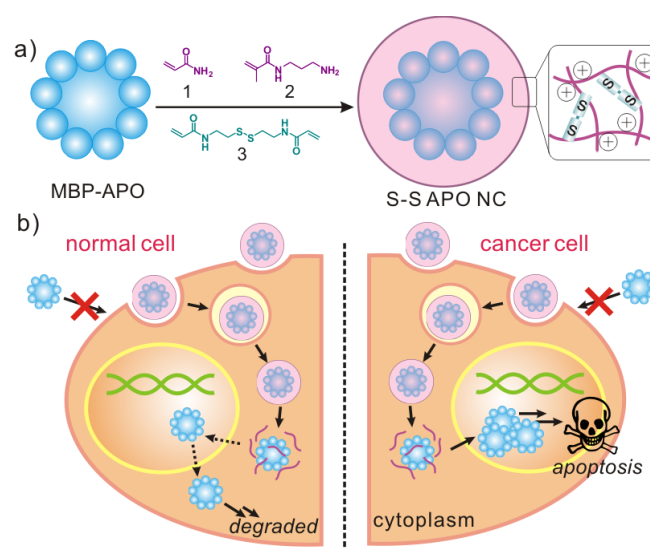
Figure 1. Schematic diagram of synthesis of degradable apoptin nanocapsules (S-S APO NC) and delivery into tumor cells to induce apoptosis.

[*] M. Zhao, Dr. Z. Gu and Prof. Y. Tang
Department of Chemical and Biomolecular Engineering
Department of Chemistry and Biochemistry
University of California, Los Angeles
Los Angeles, CA 90095 (USA)
Fax: (+1) 310-206-4107
Phone: (+1) 310-825-9538
E-mail: yitang@ucla.edu

B. Hu, Dr. K.I. Joo and Prof. P. Wang
Mork Family Department of Chemical Engineering and
Materials Science, University of Southern California
Los Angeles, CA 90089 (USA)
Phone: (+1) 213-740-0780
E-mail: pinwang@usc.edu

Supporting information for this article is available on the WWW under http://www.angewandte.org or from the author.

We chose to work with maltose-binding-protein fused apoptin (MBP-APO) which can be highly expressed in soluble form from *Escherichia coli*, whereas native apoptin form inclusion bodies.[14] MBP-APO, although five times the length as native apoptin, has been shown by gel filtration to similarly assemble into a multimeric complex and to capture the essential functions and selectivity of native apoptin.[14] Nanoparticle-mediated delivery of functional MBP-APO poses unique challenges.[24] First, the protein cargo preassembles into large complexes with an average diameter of ~ 40 nm and molecular weight of ~ 2.4 MDa.[14] To achieve nanoscale sizes that are optimal for *in vivo* administration (~100 nm),[25] a loading strategy that leads to compact particles is preferred. Second, in order to maintain the noncovalent multimeric state of functional MBP-APO, the protein loading and release processes need to take place under very mild, physiological conditions in the absence of surfactants. The globular and undefined nature of the protein further complicates the preparation process. Lastly, the protein cargo must be released into the cytoplasm in its native functional form to retain tumor selectivity, including the native spatial presentation of nuclear localization/export signals, as well as the phosphorylation site and

downstream signalling elements within apoptin.

Based on these challenges and requirements, we selected to use a polymeric nanocapsule approach[26] in which the MBP-APO complex is nearly individually and noncovalently protected in a water soluble polymer shell (Figure 1). This slightly positively-charged shell protects the MBP-APO from serum proteases and harsh environment, as well as enables cellular uptake through endocytosis.[27] The polymeric layer is weaved together by redox-responsive crosslinker that can be degraded once the nanocapsules are exposed to the reducing environment in cytoplasm. The noncovalent nature of the polymer shell ensures completely reversible encapsulation and release of native protein in the cell.
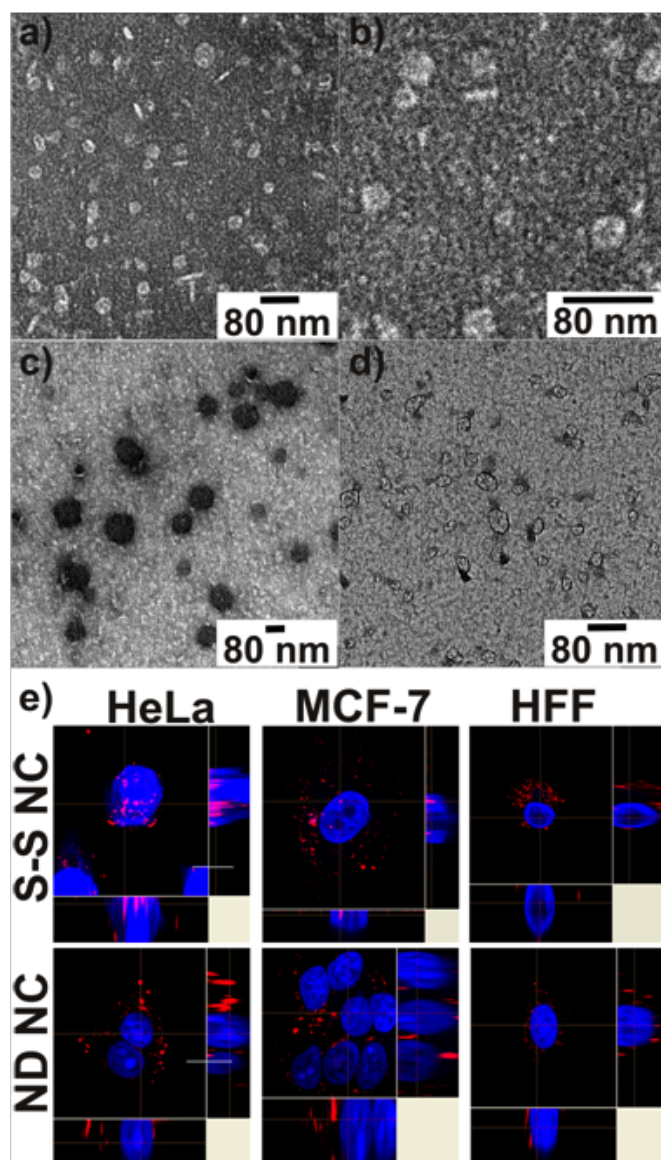
Figure 2. S-S APO NC characterization and cellular localization. TEM images of a) native MBP-APO; (b) enlarged image of MBP-APO; (c) S-S APO NC; and (d) degraded S-S APO NC after treatment with 2mM GSH for 6 hours at 37°C; (e) confocal microscopy of cellular localization of rhodamine-labeled MBP-APO encapsulated in redox-responsive (S-S NC) and nondegradable NC (ND NC) to cancer cell lines HeLa and MCF-7 and noncancerous HFF. Nuclei were stained with DAPI (blue). The scale bar is 20 µm.
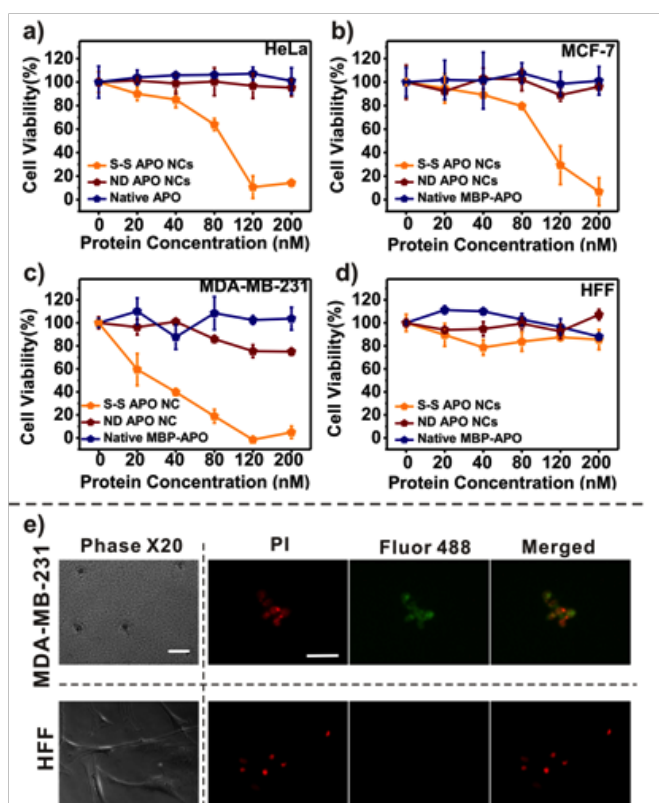
MBP-APO (pI = 6.5) was first purified from *E. coli* extract using an amylose-affinity column (See Supporting Information,

Figure S1). Dynamic Light Scattering (DLS) measurement revealed an average hydrodynamic radius of 36.1 nm (distribution shown in Figure S2), consistent with that of the reported for the MBP-APO complex.[14] Transmission Electron Microscopy (TEM) analysis of MBP-APO showed similarly sized protein complexes (Figure 2a and enlarged in Figure 2b). Interestingly, MBP-APO complexes appear to adopt a disk-shaped structure despite the lack of defined secondary structure from the apoptin component. Since the apoptin portion of the protein can self-assemble into the ~40-mer complex, we propose a three dimensional arrangement of MBP-APO in which the *C*-terminal apoptin forms the central spoke of the wheel-like structure (Figure 1), with the larger MBP portion distributed around on the edge. The planar arrangement allows the apoptin portion of the fusion protein to remain accessible to its protein partners, which may explain how the MBP-APO fusion retains essentially all of the observed functions of free apoptin.

Following electrostatic deposition of the monomers acrylamide (**1** in Figure 1a) and *N*-(3-aminopropyl)methacrylamide (**2**), and the crosslinker *N,N'*-bis(acryloyl)cystamine (**3**), at a molar ratio of 12:9:1, onto MBP-APO (1 mg) in carbonate buffer (5 mM, pH 9.0), *in situ* polymerization was initiated with the addition of free radical initiators and proceeded for one hour. The molar ratio reported is optimized to minimize protein aggregation and precipitation, as well as to maximize the solution stability of the nanocapsule formed (S-S APO NC). Excess monomers and crosslinkers were removed using ultrafiltration and the S-S APO NC was stored in PBS buffer (pH 7.4). DLS clearly showed increase in average diameter of the sample to ~ 75 nm with a slightly positive ζ-potential value of 2.4 mV (SI Table S1). TEM analysis of the S-S NC confirmed the nearly doubling in diameter of the spherical particle (Figure 2c). Unexpectedly, the NCs displayed dark contrast upon uranyl acetate staining not typically observed with polymeric particles, which hints the cores of the particles are very densely packed. As expected of the redox-responsive crosslinkers, the reduction of nanocapsule size to essentially that of the native MBP-APO can be seen upon treatment of the reducing agent glutathione (2 mM GSH, 6 hours 37°C). As shown in Figure 2d, the densely packed NCs were completely dissociated into particles (~30 nm) that resemble those seen in Figure 2a, confirming the reversible nature of the encapsulation process. In contrast, the densely packed MBP-APO nanocapsules crosslinked with the nondegradable crosslinker *N,N'*-methylene bisacrylamide (ND APO NC) were not degraded in the presence of GSH (data not shown).
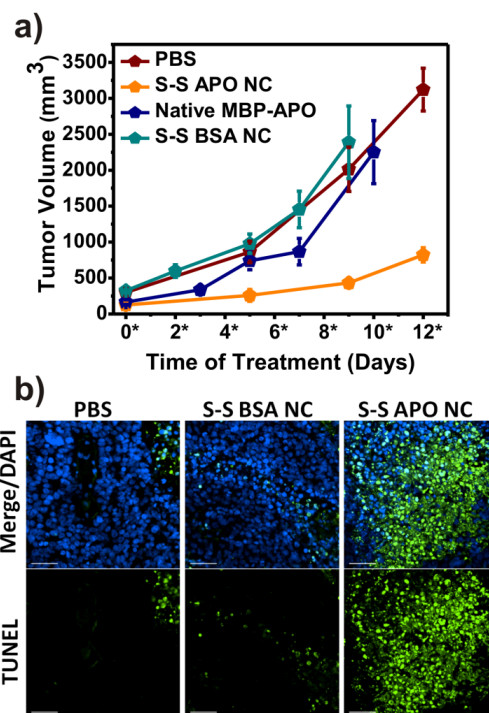
After demonstrating the *in situ* polymerization strategy can reversibly wrap the large MBP-APO complex, we next examined the cellular uptake of the S-S APO NC and its cellular localization. If the unique tumor selectivity of MBP-APO is maintained following the encapsulation and releases processes, we expect to find MBP-APO to enter the nucleus of the tumor cell, whereas in noncancerous cell it resides in the cytoplasm. Prior to the polymerization process, the native MBP-APO was conjugated to amine-reactive rhodamine (Rho-APO) (Supporting information). Subsequent encapsulation yielded similarly sized NCs. Two cancer cell lines HeLa and MCF-7, together with the human foreskin fibroblast (HFF), were treated with either S-S Rho-APO NC or ND Rho-APO NC. Fluorescent images showed all NCs readily penetrated the cell membrane and can be observed to be localized in the cytoplasm within one hour (Figure S3). To analyze protein localization using confocal microscopy, cells were fixed and the nuclei were stained with DAPI (Figure 2e). As cytotoxicity was observed with the cancer cell lines treated with S-S APO NC (see Figure 3), sub-lethal concentrations (20 nM) of the NCs were added

to imaging samples and the cells were collected before morphology changed and detachment took place. In the case of ND Rho-APO NCs, red fluorescence signals remained in the cytoplasm for all three cell lines, indicating the MBP-APO was well-shielded by the nondegradable polymeric shell and its nuclear localization signals is not accessible. In stark contrast, when HeLa cells were treated with S-S Rho-APO NC, strong red fluorescence of rhodamine was localized in the nuclei, resulting in intense pink color as a result of overlapping of rhodamine and DAPI fluroescence. Z-stacking analysis confirmed the MBP-APO to be localized inside of the nuclei (Figure 2e). Similar results were observed with MCF7 cells, although the fluorescence intensity was not as strong as in the HeLa cells. These results confirmed that the MBP-APO delivered can indeed be released in native forms inside the cytoplasm and enter the nuclei. More importantly, the specificity of MBO-APO delivered towards cancer cell lines were demonstrated in the confocal image of noncancerous HFF cells treated with S-S Rho-APO NC, as all of the dye signals remained in the cytosol and no nuclear accumulation can be observed.

We then investigated whether the MBP-APO protein delivered still possess its function to induce tumor-selective apoptosis. The potency and selectivity of S-S APO NCs was tested on cancer cell lines HeLa, MCF-7, MDA-MB-231, and the HFF (Figure 3a). MTS assay was used to measure cell viability 48 hours after addition of the protein and NCs. For each cell line, ND APO NC and native MBP-APO were used as negative controls. When S-S APO NC was added to a final concentration of 200 nM, all three cancer cell lines had no viable cells, whereas remarkably ~75 % of the HFF had survived. The IC_{50} values were 80 and 30 nM for HeLa and MDA-MB-231, respectively. The IC_{50} for MCF-7 was notably higher at ~100 nM, which may be due to the deficiency in the terminal executioner CP-3 and reliance on other effector caspases for apoptosis.[28,29] As expected, native MBP-APO and ND APO NC did not notably decrease the viability of any these cell lines tested, consistent with the inability to enter cells and release MBP-APO, respectively. The morphologies of MDA-MB-231 and HFF cells were examined under after the various treatments. Only the S-S MBP-APO NC treated MDA-MB-231 cells exhibited blebbing and shrinkage, which are hallmarks of apoptotic cell death (Figure 3b and Figure S4). Using TUNEL assay, only S-S MBP-APO NC treated MDA-MB-231 showed nuclear fragmentation associated with apoptosis (Fluor 488), whereas all other samples, native MBP-APO, ND APO NC at the same concentration, as well as HFF treated with 200 nM S-S APO NC had no sign of apoptosis (Figure S4). Collectively, these results demonstrate the released MBP-APO upon degradation retains the potency and selectivity as the transgenically expressed apoptin in previous studies.[9]

Figure 3. Cytotoxicity and apoptosis observed following S-S APO NC treatment. (a) HeLa; (b) MCF-7; (c) MDA-MB-231; or (d) HFF cells with treatment of different concentrations of S-S APO NC, ND APO NC, and native MBP-APO (e) Apoptosis induced by S-S APO NC determined by TUNEL assay. Images on the left are bright field microscopy images of MDA-MB-231 and HFF cells treated for 24 hours with 200 nM S-S APO NC. The scale bar represents 50 μm; Images right of the dash line shows detection of apoptotic fragmentation of the nucleosome after same treatment using APO-BrdU[TM] TUNEL assay. The scale bar represents 50 μ m. Red fluorescence represents the propidium-iodide-stained total DNA, and green fluorescence represents the Alexa Fluor 488-stained nick end label, the indicator of apoptotic DNA fragmentation. The merged pictures combine the PI-stained nuclei and the Alexa Fluor 488-stained nick end label. (Note the bright field images do not overlap with the fluorescent images; cells were detached and collected for TUNEL assay after treatment).

Figure 4. Treatment of S-S APO NC results in tumor growth retardation through apoptosis. a) Significant tumor inhibition was observed in the mice treated by S-S APO NC. Female athymic nude mice were subcutaneously grafted with MCF-7 cells and treated with intratumoral injection of MBP-APO (n=4) or S-S APO NC (n=4) (200 μg apoptin/mouse) every other day. PBS (n=3) and S-S BSA NC (n=4) were included as negative controls. The average tumor volumes were plotted vs. time. Asterisks indicate injection days. b) Detection of apoptosis in tumor tissues after treatment with different NC. Cross-sections of MCF-7 tumors were stained with fluorescein-dUTP (green)

for apoptosis and DAPI for nucleus (blue). The scale bars represent 50 μm.

Having demonstrated that S-S APO NC is highly effective in killing various tumor cell lines *in vitro*, we further examined its potency in mouse xenograft model. Female athymic nude (*nu/nu*) mice were subcutaneously grafted on the back flank with 5×10^6 MCF-7 breast cancer cells. When the tumor volume reached 100-200 mm^3 (day 0), mice were randomly separated into different groups and treated with intratumoral injection of PBS, MBP-APO, S-S APO NC. In addition, S-S BSA (bovine serum albumin) NC as added as a nonlethal protein cargo control testing the effects of the S-S NC capsule components on tumor cells in vivo. Tumors treated with saline or S-S BSA NC expanded rapidly and reached the maximum limit (>2500 mm^3) within 12 days. In sharp contrast, tumor growth was significantly delayed when treated with S-S APO NC. The native MBP-APO showed negligible tumor inhibition in the treated group over time, which was consistent with the *in vitro* study results. Fixed tumor tissues collected from each treatment group was examined for DNA fragmentation using *in situ* TUNEL assay. The images revealed the highest level of cell apoptosis for the tumor harvested from mice treated with S-S APO NC, correlating well with the significantly delayed tumor growth observed for this treatment group and confirming that tumor growth inhibition was indeed due to apoptin-mediated apoptosis. The observed high-degree apoptosis indicates that in addition to tumor cell killing directly caused by uptake of apoptin, the dying cells can lead to a possible bystander killing effect on surrounding tumor cells, which may increase overall therapeutic effect of S-S APO NC. The xenograft study verified that the S-S NC effectively delivered MBP-APO proteins to tumor cells *in vivo* and significantly slowed down tumor progression.

In conclusion, we were able to deliver the high molecular weight complex of the tumor-selective MBP-APO using a redox degradable polymeric nanocapsule in vitro and in vivo. The choice and design of the nanocapsule is well-suited for diverse protein targets because its mild preparation conditions, completely reversible encapsulation and efficient cell membrane penetration/release of the protein cargo in the cytoplasm. Our application here further illustrates how intracellular protein delivery using nanoscale system can provide new possibilities for achieving selective cancer therapy.

[1]   J. B. Gibbs, *Science* **2000**, *287*, 1969-1973.
[2]   J. H. Atkins, L. J. Gershell, *Nat Rev Drug Discov* **2002**, *1*, 491-492.
[3]   G. I. Evans, K. H. Vousden, *Nature*, **2001**, *411*, 342-348.
[4]   J. C. Reed, *Cancer Cell*, **2003**, *3,* 17-22.
[5]   T. G. Cotter, *Nat. Rev. Cancer,* **2009**, *9*, 501-507.
[6]   A. Russo, M. Terrasi, V. Agnese, D. Santini, V. Bazan, *Ann Oncol* **2006**, *17*, 115-123.
[7]   C. J. Brown, S. Lain, C. S. Verma, A. R. Fersht, D. P. Lane, *Nat. Rev. Cancer,* **2009**, *9*, 862-873.
[8]   M. H. M. Noteborn, *Euro. J. Pharmacol.* **2009**, *625*, 165-173.
[9]   C. Backendorf, A. E. Visser, A. G. de Boer, R. Zimmerman, M. Visser, P. Voskamp, Y. H. Zhang, M. Noteborn, *Annu. Rev. Pharmacol. Toxicol.* **2008**, *48*, 143-169.
[10]   M. Los, S. Panigrahi, I. Rashedi, S. Mandal, J. Stetefeld, F. Essmann, K. Schulze-Osthoff, *Biochim. Biophys. Acta.* **2009**, *1793*, 1335-1342.
[11]   S. M. Zhuang, A. Shvarts, H. van Ormondt, A. G. Jochemsen, A. J. van der Eb, M. H. Noteborn, *Cancer Res* **1995**, *55*, 486-489.
[12]   J. G. Teodoro, D. W. Heilman, A. E. Parker, M. R. Green, *Genes Dev.* **2004**, *18*, 1952-1957.
[13]   A. A. A. M. Danen-Van Oorschot, D. F. Fischer, J. M. Grimbergen, B. Klein, S. M. Zhuang, J. H. F. Falkenburg, C. Backendorf, P. H. A. Quax, A. J. Van der Eb, M. H. M. Noteborn, *Proc Natl Acad Sci USA* **1997**, *94*, 5843-5847.
[14]   S. R. Leliveld, Y. H. Zhang, J. L. Rohn, M. H. Noteborn, J. P. Abrahams, *J Biol. Chem.* **2003**, *278*, 9042-9051.
[15]   A. A. A. M. Danen-Van Oorschot, Y. H. Zhang, S. R. Leliveld, J. L. Rohn, M. C. M. J. Seelen, M. W. Bolk, A. van Zon., S. J. Erkeland, J. P. Abrahams, D. Mumberg, M. H. M. Noteborn, *J. Biol. Chem.,* **2003**, *278,* 27729-27736.
[16]   J. L. Rohn, Y. H. Zhang, R. I. Aalbers, N. Otto, J. Den Hertog, N. V. Henriquez, C. J. Van De Velde, P. J. Kuppen, D. Mumberg, P. Donner, M. H. Noteborn, *J. Biol. Chem.* **2002**, *277*, 50820-50827.
[17]   A. M. Pietersen, M. M. van der Eb, H. J. Rademaker, D. J. van den Wollenberg, M. J. Rabelink, P. J. Kuppen, J. H. van Dierendonck, H. van Ormondt, D. Masman, C. J. van de Velde, A. J. van der Eb, R. C. Hoeben, M. H. Noteborn, *Gene Ther* **1999**, *6*, 882-892.
[18]   M. M. van der Eb, A. M. Pietersen, F. M. Speetjens, P. J. Kuppen, C. J. van de Velde, M. H. Noteborn, R. C. Hoeben, *Cancer Gene Ther.* **2002**, *9*, 53-61.
[19]   D. J. Peng, J. Sun, Y. Z. Wang, J. Tian, Y. H. Zhang, M. H. Noteborn, S. Qu, *Cancer Gene. Ther.* **2007**, *14*, 66-73.
[20]   M. L. Edelstein, M. R. Abedi, J. Wixon, *J. Gene. Med.* **2007**, *9*, 833-842.
[21]   L. Guelen, H. Paterson, J. Gaken, M. Meyes, F. Farzaneh, M. Tavassoli, *Oncogene*, **2004**, *23*, 1153-1165.
[22]   J. Sun, Y. Yan, X. T. Wang, X. W. Liu, D. J. Peng, M. Wang, J. Tian, Y. Q. Zong, Y. H., Zhang, M. H. M. Noteborn, S. Du, *Int. J. Cancer*, **2009**, *124*, 2973-2981.
[23]   J. Shi, A. R. Votruba, O. C. Farokhzad, R. Langer, *Nano Lett.* **2010**, *10*, 3223-3230.
[24]   Z. Gu, A. Biswas, M. Zhao, Y. Tang, *Chem. Soc. Rev.* **2011**, *40*, 3638-3655.
[25]   P. P. Adiseshaiah, J. B. Hall, S. E. McNeil, *Nanomed. Nanobi.* **2010**, *2*, 99-112.
[26]   M. Zhao, A. Biswas, B. L. Hu, K. I. Joo, P. Wang, Z. Gu, Y. Tang, *Biomaterials* **2011**, *32*, 5223-5230.
[27]   Z. Gu , M. Yan, B. Hu, K. I. Joo, A. Biswas, Y. Huang, Y. Lu, P. Wang, Y. Tang, *Nano Lett.* **2009**, *9*, 4533-4538.
[28]   M. Burek, S. Maddika, C. J. Burek, P. T. Daniel, K. Schulze-Osthoff, M. Los, *Oncogene* **2006**, *25*, 2213-2222.
[29]   R. U. Janicke, M. L. Sprengart, M. R. Wati, A. G. Porter, *J. Biol. Chem.,* **1998,** *273*, 9357-9360.

Protein Delivery

Muxun Zhao, Biliang Hu, Zhen Gu, Kye-Il Joo, Pin Wang and Yi Tang*
_____ **Page – Page**

Effcient delivery of a high molecular weight tumor-killing protein complex
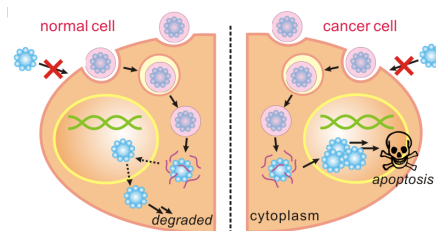
Selective Killer:

Apoptin, the tumor-selective killer, can be encapsulated into polymeric nanocapsule with redox-responsive crosslinker to achieve efficient intracellular delivery. The protein delivered can be released in its native form in cytoplasm to induce tumor-specific apoptosis and inhibition of tumor progression, as demonstrated in both *In vitro* and *in vivo* studies.

SUPPORTING INFORMATION

Efficient Delivery of a High Molecular Weight Tumor-Killing Protein Complex **
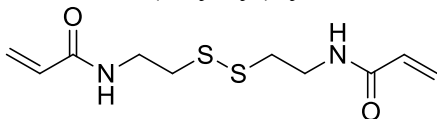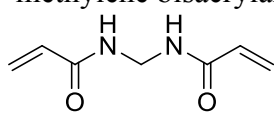
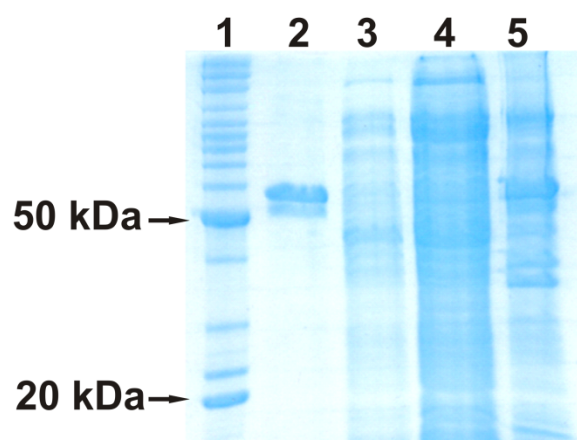*Muxun Zhao, Biliang Hu, Zhen Gu, Kye-Il Joo, Pin Wang and Yi Tang**

Contents

1. Table & Figures

Table S1. Mean hydrodynamic size and ζ- potential of protein NCs

|	S-S APO NC	S-S BSA NC	ND APO NC
Size (nm)	74.71	10	79.58
ζ-poteintial (mV)	2.4±0.4	4.7±0.4	1.6±0.4
Crosslinker	*N,N'*-bis(acryloyl)cystamine		*N,N'*-methylene bisacrylamide

Figure S1. SDS-PAGE for denatured MBP-APO samples. Lane 1 Molecular weight marker; Lane 2 Purified MBP-APO; Lane 3 Wash fraction; Lane 4 Unbounded cell lysate proteins; Lane 5 Insoluble pellet dissolved in 8M urea
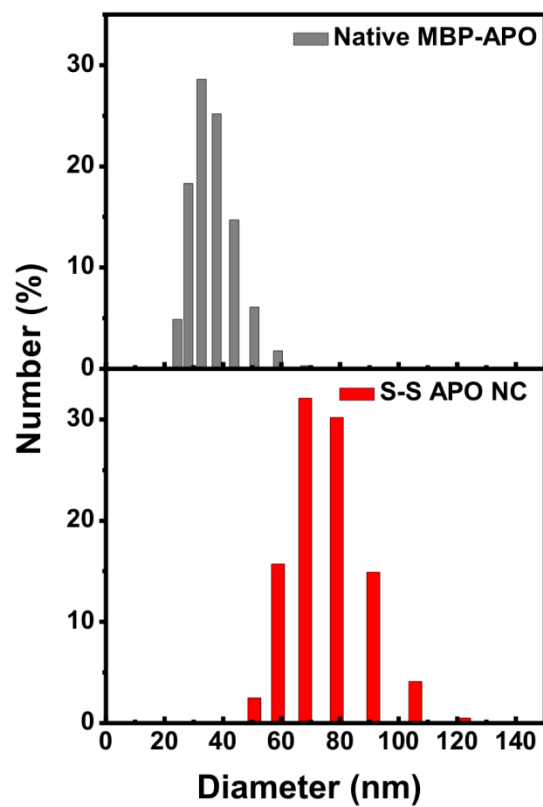
Figure S2 Size distribution of native MBP-APO and S-S APO NC formed. The hydrodynamic sizes of the native MBP-APO (grey) and S-S APO NC (red) were determined by DLS.

S-S Rho-APO NC **ND Rho-APO NC**

a) b)

1 hr

c) d)

24 hr
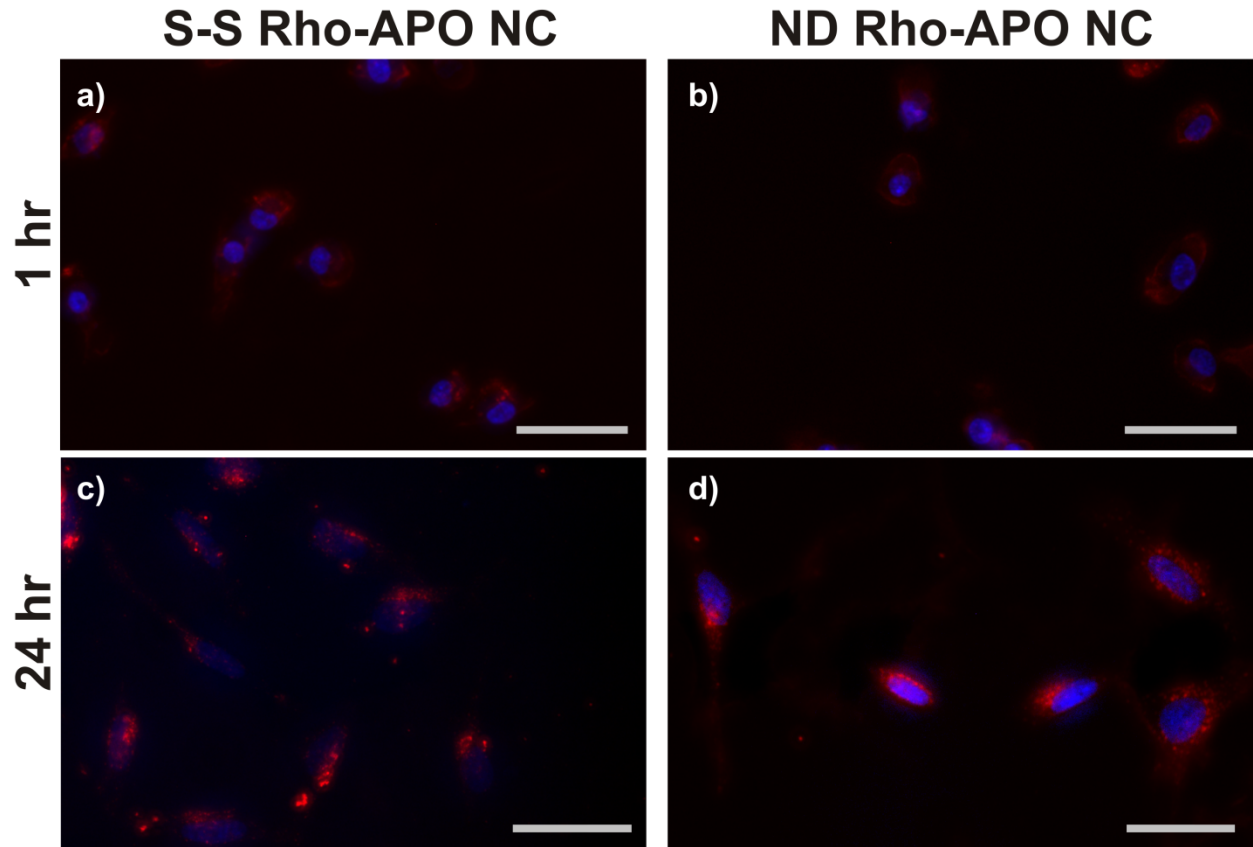
Figure S3 Internalization of S-S APO NC and ND APO NC. Fluorescence microscope images of MDA-MB-231 cells after 1 and 24 hours incubation with 20 nM S-S Rho-APO NCs and with 20 nM ND Rho-APO NCs. Nuclei were stained with DAPI. The scale bar represents 50 μm
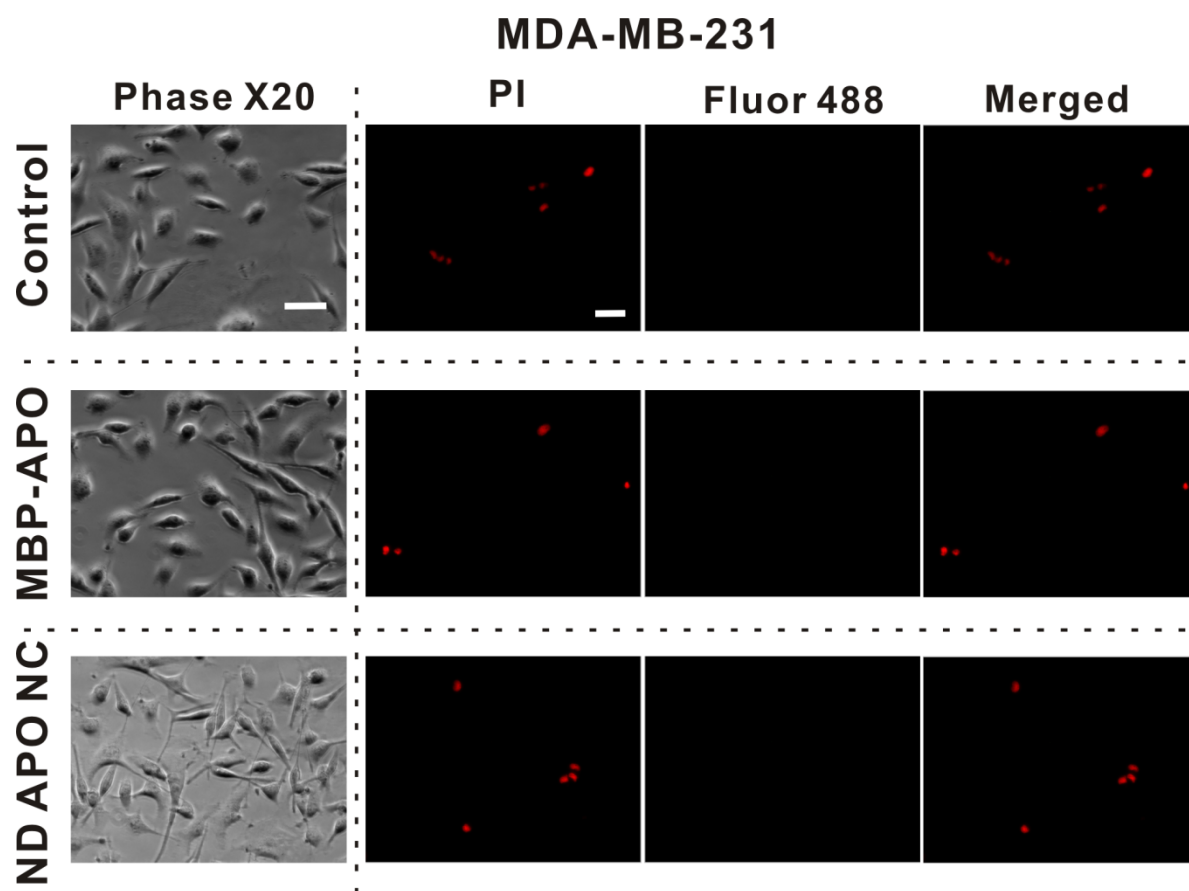
Figure S4 MDA-MB-231 cells TUNEL assay control groups. Left images of dash line are Bright-field-microscopy images of MDA-MB-231 treated for 24 hours with (i) control (saline); (ii) 200 nM native MBP APO; (iii) 200 nM ND APO NC. The scale bar represents 50 µm; Imagines right of dash line are apoptotic fragmentation of the nucleosome detected by APO-BrdUTM TUNEL after same treatment as above. The scale bar represents 50 µm. Red fluorescence represents the propidium-iodide-stained total DNA, and Alexa Fluor 488 represents apoptotic DNA fragmentation. The merged pictures combine the PI-stained nuclei and the Alexa Fluor 488-stained nick end label. Note the bright field images do not overlap with the fluorescent images.

2. Experimental Section

2.1 Materials

N-(3-aminopropyl) methacrylamide hydrochloride was purchased from Polymer Science, Inc. CellTiter 96® AQueous One Solution Cell Proliferation Assay (MTS) reagent was purchased from Promega Corporation. APO-BrdU[TM] TUNEL Assay Kit was purchased from Invitrogen. In Situ Cell Death Detection Kit, POD; was purchased from Roche Applied Science. Female athymic nude (nu/nu) mice, 6 weeks of age, were purchased from Charles River Laboratories (Wilmington, MA). All other chemicals were purchased from Sigma-Aldrich and used as received. The deionized water was prepared by a Millipore NanoPure purification system (resistivity higher than 18.2 MΩ·cm^{-1}).

2.2 Instruments

The Bradford protein assay was carried out on a Thermo Scientific GENESYS 20 spectrometer. The size distribution and ζ-potential of NCs were measured on the Malvern particle sizer Nano-ZS. Transmission electron microscopy (TEM) images were obtained using Philips EM-120 TEM instrument. Fluorescent images were taken with Zeiss Axio Observer Z1 Inverted Microscope and Yokogawa spinning-disk confocal microscope (Solamere Technology Group, Salt Lake City, UT) on Nikon eclipse Ti-E Microscope equipped with a 60×1.49 Apo TIRF oil objective and a Cascade II: 512 EMCCD camera (Photometrics). An AOTF (acousto-optical tunable filter) controlled laser-merge system (Solamere Technology Group Inc.) was used to provide illumination power at each of the following laser lines: 491 nm, 561 nm, and 640 nm solid state lasers (50 mW for each laser).

2.3 Methods

2.3.1 Protein Expression and Purification

The pMalTBVp3 plasmid for expression of the MBP-APO was a generous gift from Dr.C.Backendorf and Dr. M. Noteborn (Universiteit Leiden). MBP-APO plasmid was transformed into *Escherichia coli* BL21(DE3) cells and incubated at 37 °C overnight on LB agar plate with 100 μg/mL ampicillin. Colonies were picked and grown overnight at 37 °C with shaking (250 rpm) in 5 mL ampicillin-containing LB media. Overnight cultures were then inoculated in 500 mL of TB media with 100 μg/mL ampicillin and allowed to grow under 37 °C until the absorbance of cell density (OD$_{600}$) reached 1.0. Isopropyl *β*-D-1-thiogalactopyranoside (IPTG) was added to a final concentration of 0.1 mM to induce protein expression. After overnight incubation at 16 °C, the *E. coli* cells were harvested by centrifugation (2,000 g, 4 °C, 15 min). Cell pellets were then resuspended in 30 mL lysis buffer (25 mM Tris-HCl, 500 mM NaCl, 10% glycerol pH 7.4) and lysed by sonication. Cell debris and insoluble proteins were removed by centrifugation (17,000 rpm, 4 °C, 30 min), followed by filtering through 0.22 μm filters to fully cleare cell lysate. Afterwards, the protein was then purified on an amylase column (New England BioLabs), which was passed over 5 times with lysate under gravity flow at 4 °C then washed with wash buffer (20 mM Tris-HCL, 50mM NaCl, 1 mM EDTA, pH 7.4) to remove unbounded protein. MBP-APO was eluted from the column with 10 mM maltose buffer and buffer exchanged into PBS. The protein concentration was qualitatively assessed by SDS-PAGE and quantitatively determined by the Bradford protein assay using bovine serum albumin (BSA) as the standard.

2.3.2 NC preparation

The concentration of protein was diluted to 1 mg/mL with 5 mM sodium bicarbonate buffer at pH 9. Then 200 mg/mL acrylamide (AAm) monomer was added to 1 mL of protein solution with stirring at 4 °C. After 10 min, the second monomer, *N*-(3-aminopropyl) methacrylamide (APMAAm), was added while stirring. Different cross-linkers, *N,N'*-methylene bisacrylamide for ND NC and *N,N'*-bis(acryloyl)cystamine for S-S NC, was added 5 min after the addition of APMAAm. The polymerization reaction was immediately initiated by adding 30 μL of ammonium persulfate (100 mg/mL, dissolved in deoxygenated and deionized water) and 3 μL of *N,N,N',N'*-tetramethylethylenediamine. The polymerization reaction was allowed to proceed for 60 min. The molar ratio of AAm/APMAAm/cross-linker was adjusted to 12:9:1. Buffer exchange with phosphate-buffered saline (PBS) buffer (pH 7.4) was used to remove the remaining monomers and initiators. Rhodamine-tagged MBP-APO NCs was obtained through encapsulation of MBP-APO modified with 5-Carboxy-X-rhodamine *N*-succinimidyl ester (mass ratio (MBP-APO: rhodamine): 4:1).

2.3.3 Characterization of APO NCs

The mean hydrodynamic size and zeta potential of NCs was determined by dynamic light scattering (DLS) in PBS buffer. Samples of NCs (0.05 mg/mL) for TEM imaging were negatively stained with 2 % uranyl acetate in alcoholic solution (50 % ethanol). The lamella of stained sample was prepared on carbon-coated electron microscopy grids (Ted Pella, Inc.).

2.3.4 Cellular uptake and localization

MDA-MB-231, HeLa, MCF-7, and HFF cells (ATCC, Manassas, VA) were cultured in Dulbecco's Modified Eagle's Media (DMEM) (Invitrogen) supplemented with 10 % bovine growth serum (Hyclone, Logan, UT), 1.5 g/L sodium bicarbonate, 100 μg/mL streptomycin and 100 U/mL penicillin, at 37 °C with 98 % humidity and 5 % CO_2. To visualize NCs uptake, MDA-MB-231 cells were seeded into 48-well plate, with a density of 5,000 cells/well in 250 μL of media with supplements. Once the confluency of 80% was reached, S-S Rho-APO NC and ND Rho-APO NC were added to a final concentration of 20 nM. After 1 hour and 24 hours of incubation, cells were washed with PBS twice, stained with DAPI Nucleic Acid Stain (Invitrogen) and imaged. To determine the cellular localization of protein delivered, confocal images were taken with HeLa, MCF-7, or HFF cells incubated with 20nM of S-S Rho-APO NC or ND Rho-APO NC at 37°C for 24 h. Nuclei were then counterstained with DAPI. The Z stack images of cells were imaged at 0.4-μm intervals and analyzed by Nikon NIS Element software. Fluorescence images were acquired on a Yokogawa spinning-disk confocal scanner system (Solamere Technology Group, Salt Lake City, UT) using a Nikon eclipse Ti-E microscope equipped with a 60×/1.49 Apo TIRF oil objective and a Cascade II: 512 EMCCD camera (Photometrics, Tucson, AZ, USA). An AOTF (acousto-optical tunable filter) controlled laser-merge system (Solamere Technology Group Inc.) was used to provide illumination power at each of the following laser lines: 491 nm, 561nm, and 640 nm solid state lasers (50mW for each laser)."

2.3.5 Cytotoxicity Assay

Different cancer cells, HeLa, MCF-7 and MDA-MB-231 cells, as well as noncancerous HFF (ATCC, Manassas, VA), were seeded into 96-well plates, each well containing 5,000 cells in 100 μL of DMEM with supplements. Different concentrations of protein and NCs were added into each well and the plates were incubated at 37 °C with 98 % humidity and 5 % CO_2 for 48 hours. The cells were washed with PBS solution twice and 100 μL of fresh cell culture media with supplements was added. Then 20 μL MTS solution (CellTiter 96® AQueous One Solution Cell Proliferation Assay, Invitrogen) was added into each well and the plates were incubated for 3 hours at 37 °C. The absorbance of product was read at 490 nm using a microplate reader (PowerWave X, Bio-tek Instruments, USA).

2.3.6 *In vitro* TUNEL Assay

Apoptosis of cells was detected using APO-BrdU Terminal Deoxynucleotidyl Transferase dUTP Nick End Labeling (TUNEL) assay kit. MDA-MB-231 and HFF cells were seeded at a density of 100,000 cells/well into a 6-well plate in 2 mL of cell culture media with supplements. Proteins and NCs were added after cells covered 80 % of bottom surface. After 24 hours of incubation, cells were fixed with 1 % paraformaldehyde in PBS, followed by the addition of DNA labeling solution containing terminal deoxynucleotidyl transferase and bromodeoxyuridine (BrdUrd). Cells were then stained with Alexa Fluor® 488 dye-labeled anti-BrdUrd antibody. Samples were deposited onto slides, which were later stained with propidium iodide (PI) solution containing RNase A. Images were obtained by fluorescence microscope (Zeiss, Observer Z1) using appropriate filters for Alexa Fluor 488 and PI.

2.3.7 *In vivo* studies with MCF-7 xenograft model

All mice were housed in an animal facility at the University of Southern California in accordance with institute regulations. Female athymic nude (nu/nu) mice were subcutaneously grafted on the back flank with 5×10^6 MCF-7 tumor cells. Afterwards, tumor size was monitored by a fine caliper and the tumor volume was calculated as the product of the two largest perpendicular diameters and the vertical thickness (L×W×D, mm^3). When the tumor volume reached 100-200 mm^3, mice were randomly separated into different groups. From day 0, mice were treated with intratumoral injection of native MBP-APO or S-S APO NC (200μg per mouse) every other day. PBS and S-S BSA NC were included as the negative controls. When the tumor volume oversized 2500mm^3, the mice were euthanized by CO_2 according animal protocol. The average of tumor volume was plotted as the tumor growth curve in respective treated groups

2.3.8 Histology study

For histology study, treated tumor samples were collected and fixed in 4% paraformaldehyde, and processed for staining using the *In Situ* Cell Death Detection Kit (Roche). The stained tumor slides were observed under confocal microscope, and representative pictures were taken for analysis. Paraformaldehyde-postfixed frozen tumor sections (5-μm thick) were permeabilized with 0.1% triton X-100 and stained with a TUNEL assay kit (In Situ Cell Death Detection Kit, POD; Roche Applied Science, Indianapolis, IN) in accordance with the manufacturer's instructions. DAPI was used for nuclear counterstaining.

3. References